Springer, K.B., Pigati, J.S., Climatically driven displacement on the Eglington fault, Las Vegas Nevada. *Geology*.

This project was funded in part by the U.S. Geological Survey's Climate and Land Use Change Research and Development Program through the Paleohydrology of Desert Wetlands project. Any use of trade, product, or firm names is for descriptive purposes only and does not imply endorsement by the U.S. Government. Downloadable files of the data presented in the Data Repository can be found at doi:10.5066/P9URNORV.

Captions and References for the Data Repository files

DR 1. Composite stratigraphy and ages for sediments of the Las Vegas Formation (after Springer et al., 2018). Note that colors shown in the composite profile are intentionally intensified to differentiate between members and/or beds. Age control for the various units is based on a combination of calibrated radiocarbon ages (filled squares) and infrared-stimulated luminescence ages (filled circles). Ages reported here for the first time are shown in red; all other ages are from Springer et al. (2015; 2018).

DR 2a. Lidar image of the study area showing the Eglington fault (solid line where known; dashed line where inferred), the warp zone (shown in light gray), and the locations of the five vertical profiles shown in DR 2b. Lidar data accessed 6/12/18; online linkage: https://www.sciencebase.gov/catalog/item/4f70ab64e4b058caae3f8def. Metadata available at https://catalog.data.gov/dataset/usgs-lidar-point-cloud-lpc-nv-lasvegasvalley-2010-000085-2014-09-17-las.

DR 2b. Vertical profiles across the Eglington fault. The magnitude of displacement for each profile was determined using a minimum of 10 m of continuous surface elevation (lidar) data on both the upthrown and downthrown blocks. The slope across each interval was calculated and then extrapolated through the warp zone to determine the maximum amount of vertical separation.

DR 3. Stratigraphy, ages, and photographs of a laminated silty horizon within bed E_0 of the Las Vegas Formation near the Eglington fault that exhibits convoluted bedding, possibly the result of ground motion. The calibrated radiocarbon ages suggest this occurred in the Eglington area shortly after 19.7 ka.

DR 4a. Stratigraphy, ages, and photographs of sediments of the Las Vegas Formation that are flat-lying, undeformed, and inset 2-4 m into the incised topography of bed D_2 at two sites within the Eglington warp zone as shown in DR 4b. These calibrated ages are based on radiocarbon dating and provide an upper limit on the timing of displacement on the Eglington fault.

DR 4b. *Upper panel*: Lidar image of the study area showing the Eglington fault (solid line where known; dashed line where inferred), the warp zone (shown in light gray), and the location of a transect orthogonal to the fault (red circles) where we measured both the thickness of the exposed bed D_2 and the thickness of the inset member E deposits (DR 4a). LiDAR data accessed 6/12/18; online linkage: https://www.sciencebase.gov/catalog/item/4f70ab64e4b058caae3f8def.

Metadata available at https://catalog.data.gov/dataset/usgs-lidar-point-cloud-lpc-nv-lasvegasvalley-2010-000085-2014-09-17-las. *Lower panel*: Vertical profile based on lidar data of a transect across the Eglington fault showing the eroded cap of bed D_2 (solid gray), six different sites where we measured the current thickness of the D_2 cap (red circles), and the locations of the two stratigraphic sections shown in DR 4a (yellow stars). Based on the ages, elevations, and thicknesses of the flat-lying, undeformed member E sediments that are inset within the D_2 cap, at least 2-4 m of erosion must have occurred after fault displacement and headcutting of the surficial sediments (post-23.3 ka) but before deposition of bed E_0 (pre-19.5 ka).

DR 5. Summary of sample information, radiocarbon ages, and calibrated ages for samples collected at sites within or near the Eglington fault in our study area.

DR 6. As shown in Figure 3, a summary of slip rate calculations and uncertainties for the Eglington fault for scenarios in which displacement occurred between 27.0 and 19.5 ka (scenario 1), and between 23.3 and 19.5 ka (scenario 2). Limiting ages for scenario 1 are based on when the carbonate cap of bed D_2 hardened during D-O 4 and 3 (27.0 ka) and the age of flat-lying, undeformed sediments inset within the deformed, then incised, cap carbonate (19.5 ka). Limiting ages for scenario 2 are based on the timing of a significant drop in the water table at the onset of warming associated with D-O 2 (23.3 ka), which we hypothesize initiated movement on the fault, and the age of the inset sediments within the warp zone (19.5 ka).

DR 7. Calculations of the load removed from the Las Vegas Valley at 23.3 ka during an abrupt drop in the water table at the onset of D-O 2. Note that the magnitude of the load removed is a function of the depth to groundwater at that time. Geologic evidence confirms there was significant erosion throughout the valley between 23.5 and 23.0 ka (Springer et al., 2015; 2018). This rapid erosion indicates that the valley floor must have been largely devoid of phreatophyte plants at this time, as the presence of these plants inhibit surface flow and limit the ability of streams and flash floods to erode the fine-grained deposits. Phreatophyte plants disappear from the landscape when depth to groundwater levels exceed ~10 m (Meinzer, 1927; Morgan and Dettinger, 1996), which provides a reasonable *minimum* depth to groundwater during the centennial scale warming of D-O 2 (given as $\Delta_{t2\text{-}min}$). Assuming groundwater at this time dropped no deeper than modern levels, we can place a *maximum* constraint of ~33 m on this parameter (given as $\Delta_{t2\text{-}max}$) using the observed water-table depth of ~25 m in Las Vegas (Heilwell and Brooks, 2001), which was measured prior to the valley-wide drawdown of the water table that resulted from significant groundwater pumping in the early 20th century (Maxey and Jameson, 1948), and accounting for the stratigraphic thickness of ~8 m for the upper members of the Las Vegas Formation (Springer et al., 2018). Using an average temperature of 20 °C (Quade et al., 2003) to calculate the density of water during glacial time and a porosity of 50% for the unconsolidated sediments, we estimate the total load released by the groundwater drawdown during D-O 2 ranged from 7.11×10^{12} to 2.35×10^{13} kg, which is equivalent to a ~5-16 m deep water body across the entire 1425 km^2 of the Las Vegas Valley.

DR 8. Summary of Coulomb stress calculations over a wide range of dip angles (40-70°), coefficient of friction values (0.1-0.7), and water table drop estimates (10-33 m) for the Eglington fault. The calculations were performed using assigned values of 0.25 for Poisson's ratio, 1 for Biot's ratio, and 0.5 for porosity, which were based on the dominantly silt-sized

sediments of the Las Vegas Formation. The results (shown in Figure 4) indicate that changes in the Coulomb stress fields were sufficient in both magnitude and direction to promote displacement (as indicated by negative $\Delta\sigma_f$ values) for all dip angles when coefficient of friction values exceed 0.55. When coefficient of friction values are between 0.45 and 0.55, the results are variable and depend upon the dip angle. Displacement is inhibited for all dip angles when coefficient of friction values are less than 0.45.

References

Belyadi, H., Fathi, E., and Belyadi, F., 2019, Hydraulic Fracturing in Unconventional Reservoirs: Theories, Operations, and Economic Analysis (2nd edition), Gulf Professional Publishing, 632 p.

Bevington, P.R., and Robinson, D.K., 1992, Data Reduction and Error Analysis for the Physical Sciences (2nd edition), Boston, MA, The McGraw-Hill Companies, Inc., 328 p.

Harrill, J.R., 1976, Pumping and groundwater storage depletion in Las Vegas Valley, Nevada, 1955–1974: Nevada Department of Conservation and Natural Resources, Water Resources Bulletin, v. 44, p. 1-70.

Harris, R.A., 1998, Introduction to special section: Stress triggers, stress shadows, and implications for seismic hazard: Journal of Geophysical Research, v. 103, no. B10, p. 24,347-324,358.

Heilwell, V.M., and Brooks, L.E., 2001, Conceptual model of the Great Basin carbonate and alluvial aquifer system, U.S. Geological Survey Scientific Investigations Report 2010–5193, p. 192.

Maxey, G.B., and Jameson, C.H., 1948, Geology and water resources of Las Vegas, Pahrump, and Indian Spring Valleys, Clark and Nye Counties, Nevada: State of Nevada, Office of the State Engineer, Water Resources Bulletin 5, 121 p.

Meinzer, O.E., 1927, Large springs in the United States: U.S. Geological Survey Water-Supply Paper 557, p. 1-94.

Morgan, D.S., and Dettinger, M.D., 1996, Groundwater conditions in Las Vegas Valley, Clark County, Nevada, Part 2, Hydrogeology and Simulation of Groundwater Flow: U.S. Geological Survey Water Supply Paper, v. 2320-B, p. 1-124.

Quade, J., Forester, R.M., and Whelan, J.F., 2003, Late Quaternary paleohydrologic and paleotemperature change in southern Nevada, *in* Enzel, Y., Wells, S.G., and Lancaster, N., eds., Paleoenvironments and Paleohydrology of the Mojave and Southern Great Basin Deserts, Geological Society of America Bulletin Special Paper 368, p. 165-188.

Springer, K.B., Manker, C.R., and Pigati, J.S., 2015, Dynamic response of desert wetlands to abrupt climate change: Proceedings of the National Academy of Sciences USA, v. 112, no. 47, p. 14522-14526.

Springer, K.B., Pigati, J.S., Manker, C.R., and Mahan, S.A., 2018, The Las Vegas Formation: U.S. Geological Survey Professional Paper 1839, 62 p., p. doi: 10.3133/pp1839.

Turcotte, D.L., and Schubert, G., 2019, Geodynamics (3rd edition), Cambridge University Press, 623 p.

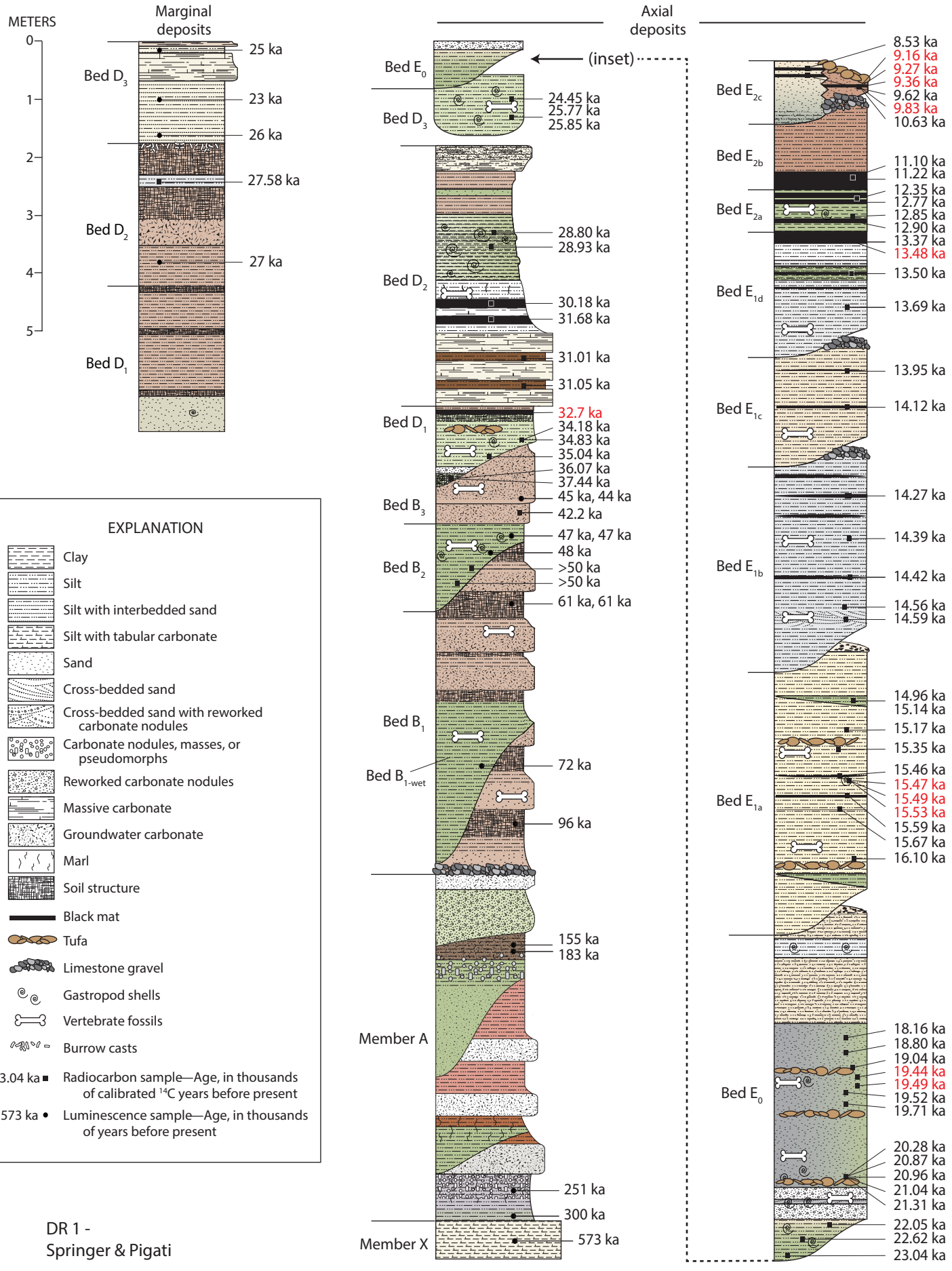

DR 1 -
Springer & Pigati

DR 2a -
Springer & Pigati

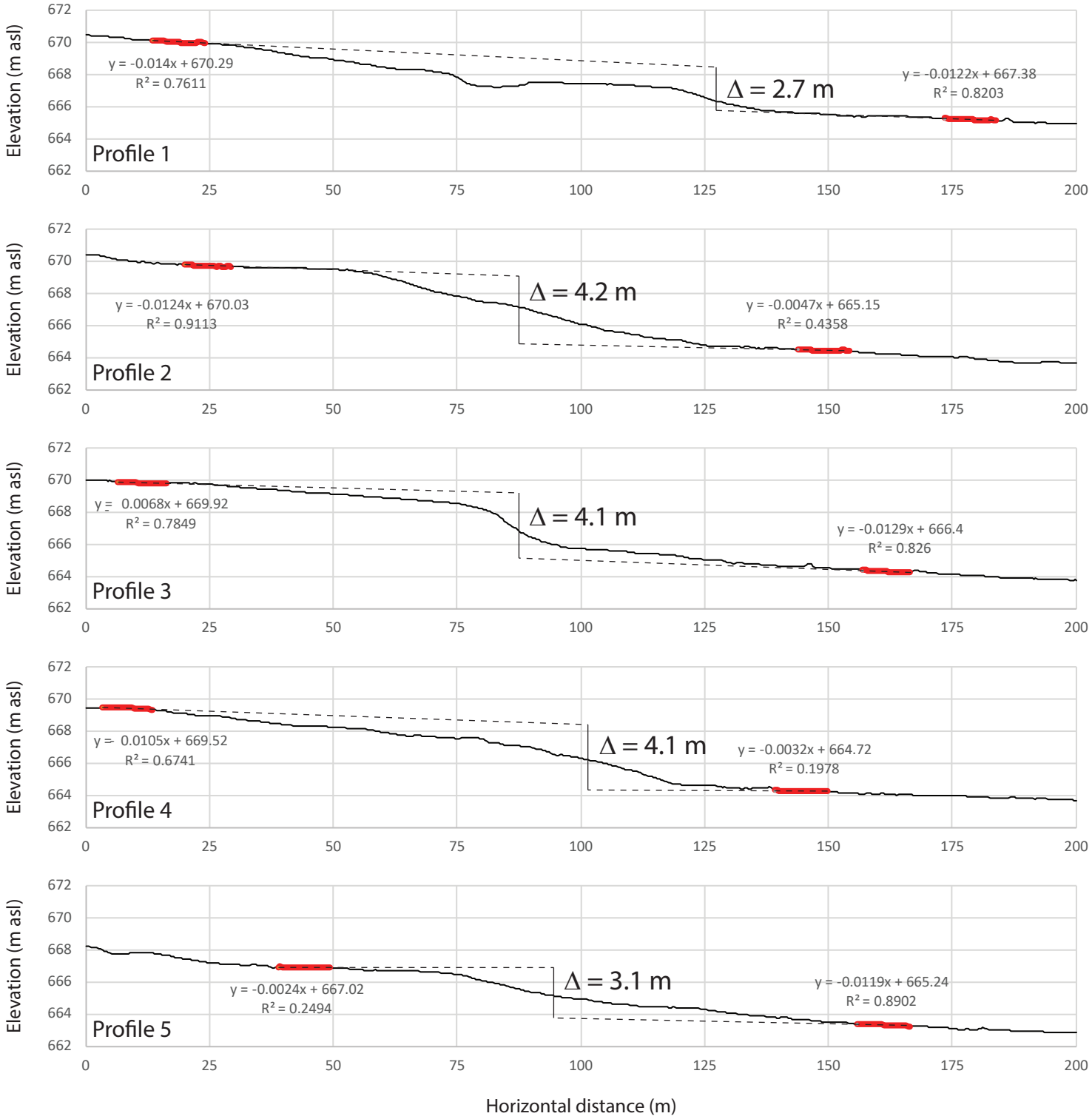

DR 2b -
Springer & Pigati

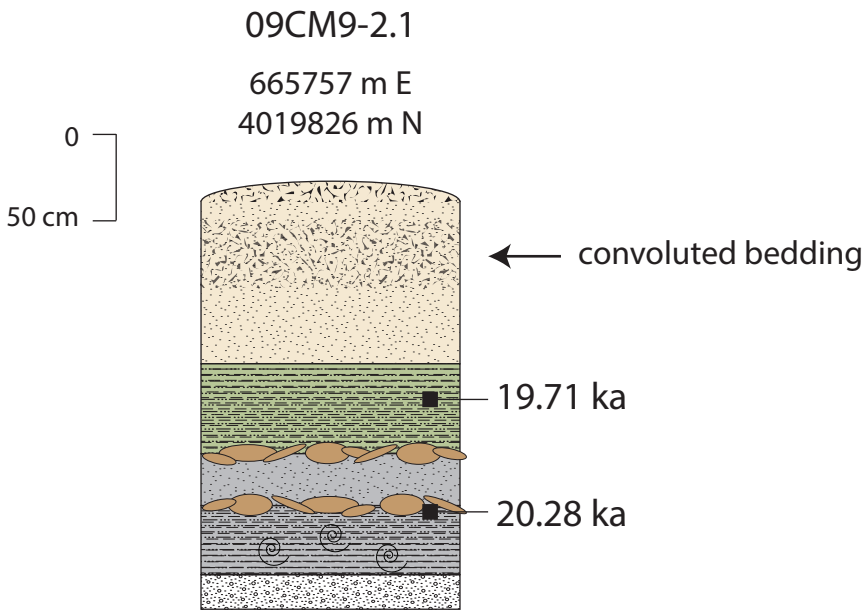

DR 3 -
Springer & Pigati

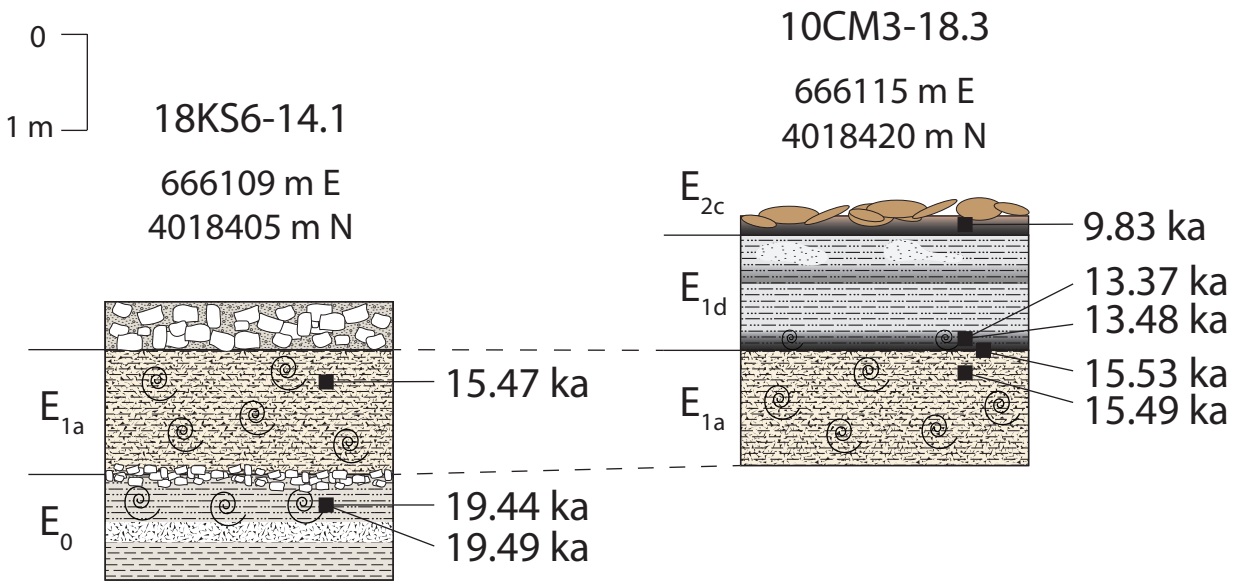

18KS6-14.1

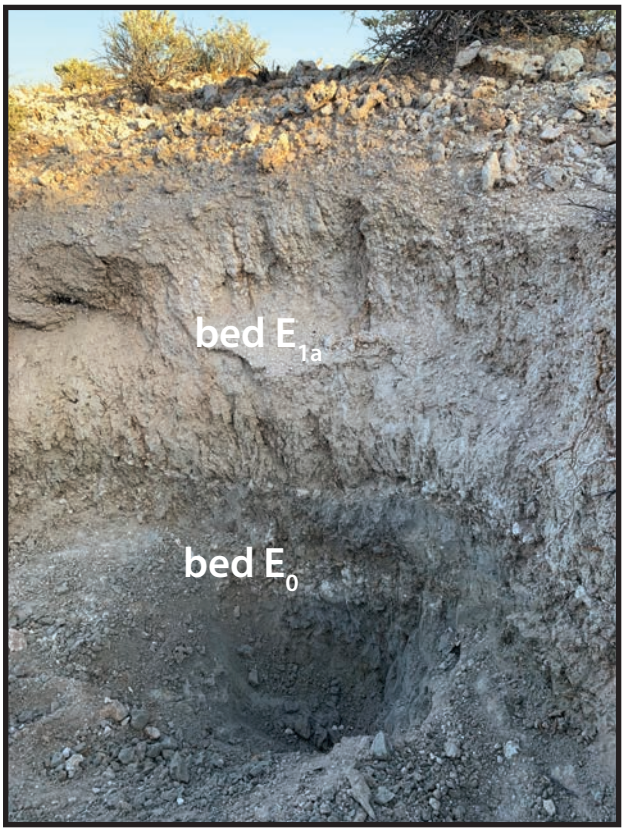

10CM3-18.3

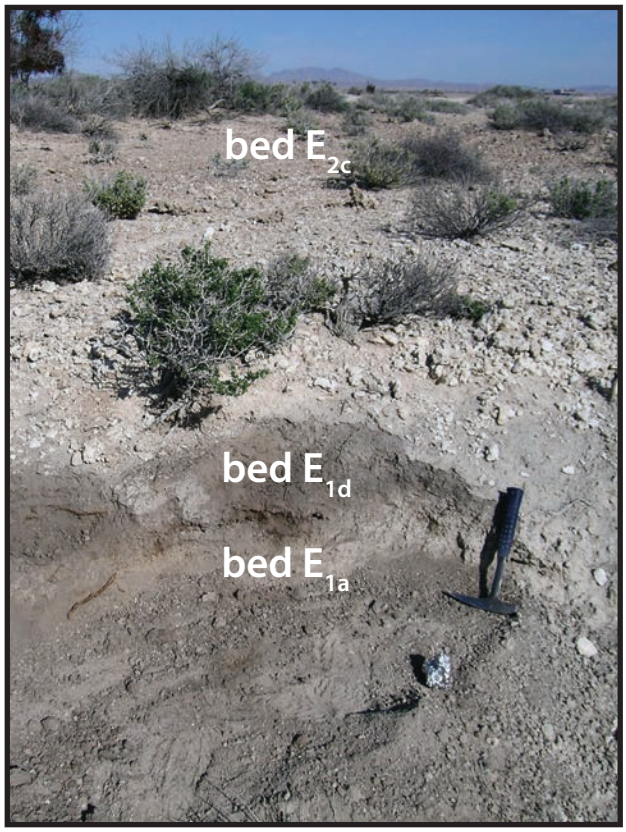

DR 4a -
Springer & Pigati

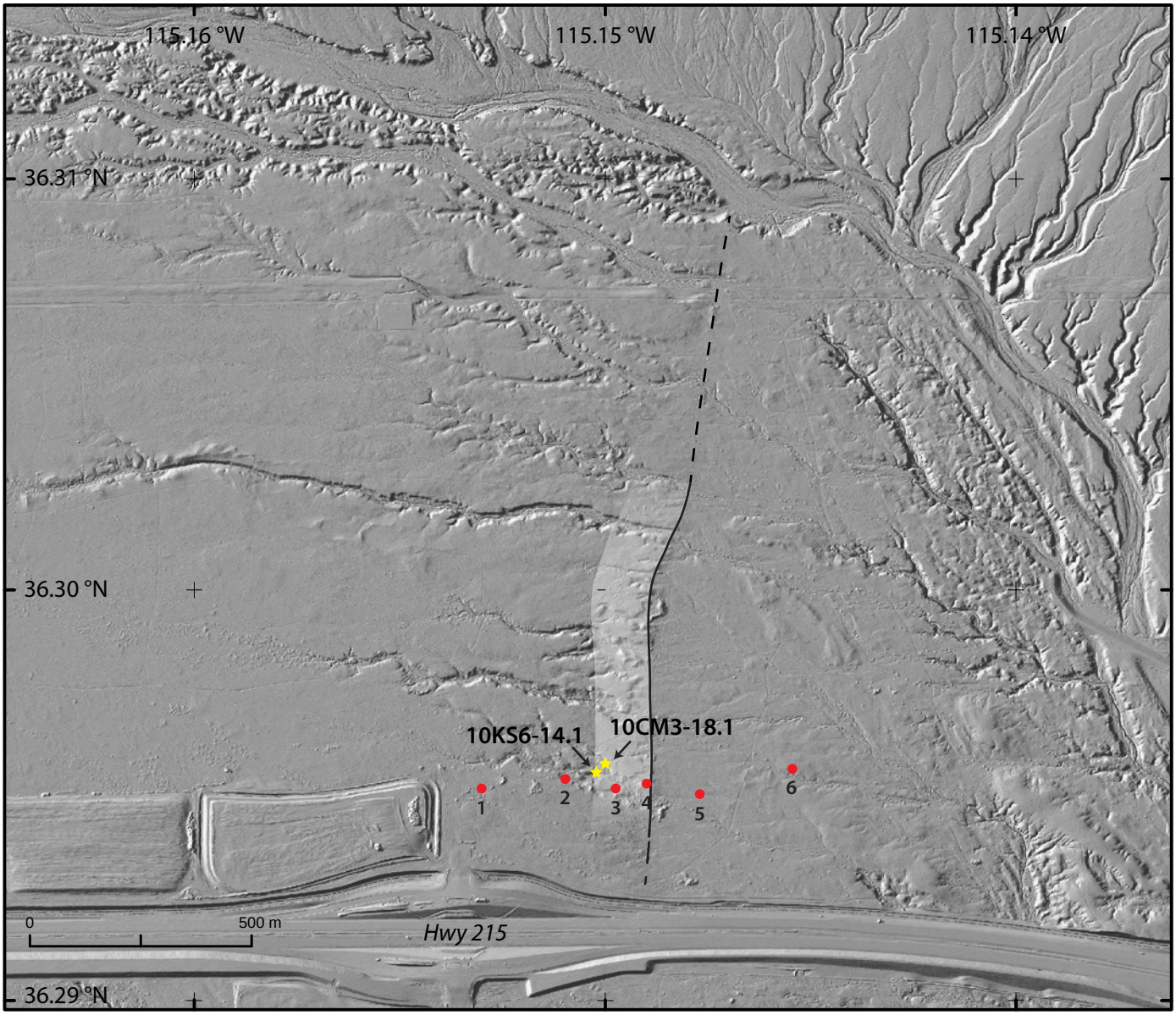

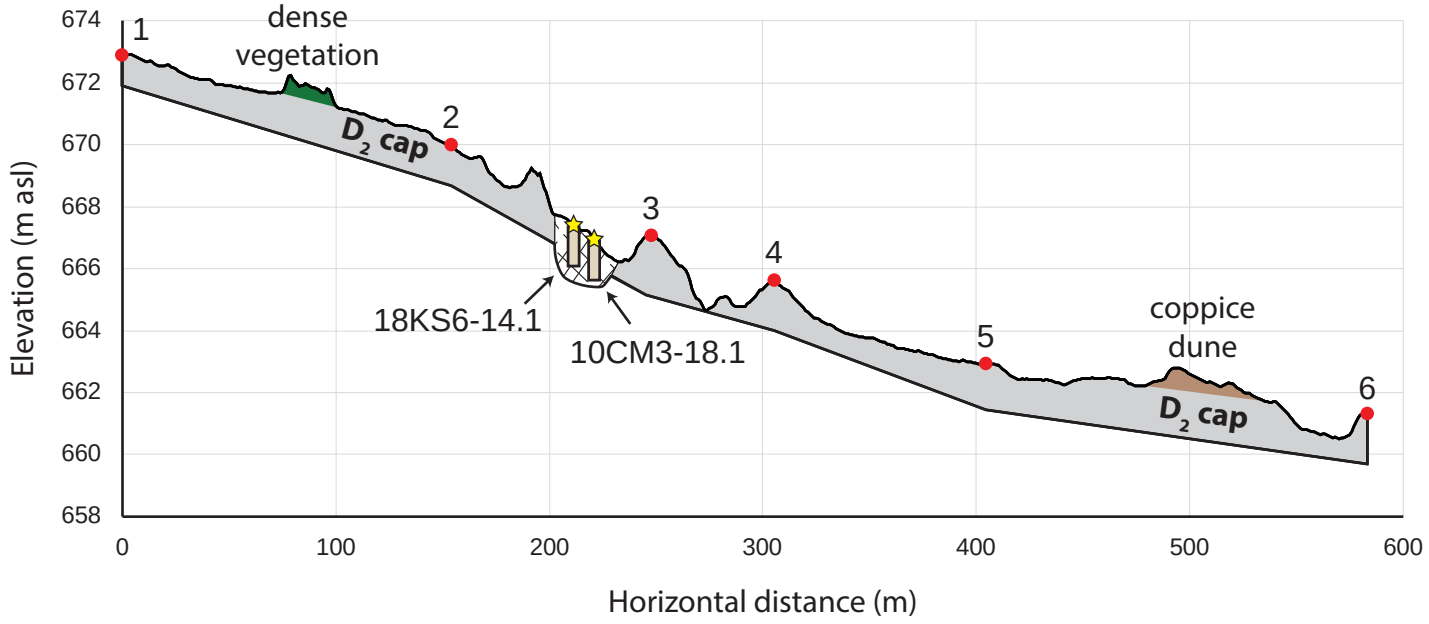

DR 4b -
Springer & Pigati

DR 5

Summary of sample information, carbon-14 ages, and calibrated ages.

Sample #	AMS #	Easting[1]	Northing[1]	Unit	Context	Material dated	Treatment[2]	^{14}C age (ka BP)	Age (cal ka BP)[3]	P[4]	Source[5]
18KS6-14.2	USGS-1105	666105	4018438	E_{2c}	black mat	organics	ABA	8.21 ± 0.04	9.16 ± 0.13	1.00	1
18KS6-15.3	USGS-1115	666114	4018434	E_{2c}	black mat	organics	ABA	8.27 ± 0.04	9.27 ± 0.14	1.00	1
18KS6-14.3	USGS-1106	665988	4018505	E_{2c}	black mat	organics	ABA	8.34 ± 0.05	9.36 ± 0.11	0.98	1
10CM3-18.3 upper	USGS-1102	666115	4018420	E_{2c}	black mat	organics	ABA	8.83 ± 0.04	9.83 ± 0.13	0.72	1
									10.01 ± 0.03	0.08	
									10.10 ± 0.05	0.20	
10CM3-18.3 lower	Beta-297878	666115	4018420	E_{1d}	black mat	charcoal	ABA	11.53 ± 0.05	13.37 ± 0.09	1.00	2
10CM3-18.3 lower (II)	USGS-1103	666115	4018420	E_{1d}	black mat	charcoal	ABA	11.67 ± 0.06	13.48 ± 0.13	1.00	1
18KS6-14.1d	USGS-1349	666109	4018405	E_{1a}	sediment	Succineidae	HCl	12.93 ± 0.07	15.47 ± 0.25	1.00	1
10CM3-18.3b	USGS-1454	666115	4018420	E_{1a}	sediment	Succineidae	HCl	12.95 ± 0.06	15.49 ± 0.23	1.00	1
10CM3-18.3a	USGS-1453	666115	4018420	E_{1a}	sediment	Succineidae	HCl	12.99 ± 0.06	15.53 ± 0.24	1.00	1
18KS6-14.1(II)	USGS-1205	666109	4018405	E_0	sediment	Succineidae	HCl	16.12 ± 0.09	19.44 ± 0.26	1.00	1
18KS6-14.1	USGS-1104	666109	4018405	E_0	sediment	Succineidae	HCl	16.16 ± 0.07	19.49 ± 0.23	1.00	1
09CM9-2.1	Beta-264965	665757	4019826	E_0	sediment	charcoal	ABA	16.30 ± 0.07	19.71 ± 0.22	1.00	2
09CM9-2.1c	Beta-272512	665744	4019833	E_0	sediment	charcoal	ABA	16.82 ± 0.07	20.28 ± 0.22	1.00	2
18KS6-14.5	USGS-1110	665869	4019435	D_1	black mat	organics	ABA	28.83 ± 0.39	32.7 ± 1.1	1.00	1

Uncertainties for the calibrated ages are given at the 2σ (95%) confidence level. All other uncertainties are given at 1σ (68%).

[1] UTM coordinates are all in zone 11S.

[2] ABA = acid-base-acid; HCl = acid leach.

[3] Calibrated ages were calculated using CALIB v.7.1html, IntCal13.14C dataset; limit 50.0 calendar ka B.P. Calibrated ages are reported as the midpoint of the calibrated range. Uncertainties are calculated as the difference between the midpoint and either the upper or lower limit of the calibrated age range, whichever is greater (reported at the 95% confidence level; 2σ). Multiple ages are reported when the probability of a calibrated age range exceeds 0.05.

[4] P = probability of the calibrated age falling within the reported range as calculated by CALIB.

[5] 1 = this study; 2 = Springer et al., 2015; 2018

DR 6
Summary of slip rate calculations.

$$v = \frac{x_1 - x_2}{t_1 - t_2}$$

Scenario 1: Displacement occurred between 27.0 and 19.5 ka

x_1 =	668.95 ± 0.10	m ASL	derived from LiDAR data; uncertainty estimated
x_2 =	664.74 ± 0.10	m ASL	derived from LiDAR data; uncertainty estimated
t_1 =	27.0 ± 0.5	ka	estimate of when D_2 cap had fully hardened (see text for details)
t_2 =	19.49 ± 0.23	ka	age of sample #18KS6-14.1 (inset sediments of bed E_0)
v =	0.6 ± 0.1	mm/yr	

Scenario 2: Displacement occurred between 23.3 and 19.5 ka

x_1 =	668.95 ± 0.10	m ASL	derived from LiDAR data; uncertainty estimated
x_2 =	664.74 ± 0.10	m ASL	derived from LiDAR data; uncertainty estimated
t_1 =	23.34 ± 0.60	ka	onset of D-O 2 (Anderson et al., 2006)
t_2 =	19.49 ± 0.23	ka	age of sample #18KS6-14.1 (inset sediments of bed E_0)
v =	1.1 ± 0.2	mm/yr	

Note: All chronologic uncertainties are given at the 2 σ (95%) confidence level.

[1] Uncertainties in v are calculated by taking the partial derivative of v with respect to each parameter (x_x,t_x), multiplying those values by their corresponding $\Delta(x_x,t_x)$ values, and summing the results quadratically (after Bevington and Robinson, 1992).

DR 7
Summary of load calculations.

$M = \rho \phi A z$

Input parameters	**Symbol**		
Density - water at 20 °C	ρ	0.9982	g / cm^3
Porosity (silt)	ϕ	50%	
Areal extent of the Las Vegas Valley[1]	A	1425	km^2
Water table depth before 23.3 ka	Δ_{t1}	0	m
Water table depth after 23.3 ka (min)	$\Delta_{t2\text{-}min}$	10	m
Water table depth after 23.3 ka (max)	$\Delta_{t2\text{-}max}$	33	m

Minimum load released	M_{min} =	7.11E+12	kg
Maximum load released	M_{max} =	2.35E+13	kg

[1] Harrill, 1976

DR 8

Summary of Coulomb stress change calculations

Input parameters	**Symbol**	**Value**		**Type**
Gravitational constant	g	9.80665	m / s^2	constant
Density - water at 20°C	ρ_w	0.9982	g / cm^3	constant
Poisson's ratio	v	0.25		assigned
Biot's ratio	α	1		assigned
Density - rock	ρ_r	2.65	g / cm^3	assigned
Porosity (silt)	φ	50%		assigned
Calculation depth[1]	z	2	km	assigned
Water table depth before 23.3 ka	Δ_{t1}	0	m	estimated
Water table depth after 23.3 ka (min)	$\Delta_{t2\text{-}min}$	10	m	estimated
Water table depth after 23.3 ka (max)	$\Delta_{t2\text{-}max}$	33	m	estimated
Dip angle (min)[2]	θ_{min}	40	degrees	variable
Dip angle (max)[2]	θ_{max}	70	degrees	variable
Coefficient of friction (min)	μ_{min}	0.1		variable
Coefficient of friction (max)	μ_{max}	0.7		variable

Calculated parameters	**Symbol**	**Value**		**Equation**
Vertical stress before 23.3 ka	$\sigma_{1\text{-}t1}$	35.777	mPa	$\sigma_1 = \rho_r(1-\vartheta)gz_r + \rho_w\vartheta g z_w$
Vertical stress after 23.3 ka (min)	$\sigma_{1\text{-}t2\text{-}min}$	35.728	mPa	
Vertical stress after 23.3 ka (max)	$\sigma_{1\text{-}t2\text{-}max}$	35.615	mPa	
Minimum pore pressure[3]	P_p	19.578	mPa	$P_p = \rho_w g z_w$
Minimum horizontal stress	$\sigma_{3\text{-}t1}$	24.978	mPa	$\sigma_3 = \frac{v}{1-v}(\sigma_1 - \alpha P_p) + \alpha P_p + \sigma_{ext}$
Minimum horizontal stress after 23.3 ka (min)	$\sigma_{3\text{-}t2\text{-}min}$	24.961	mPa	
Minimum horizontal stress after 23.3 ka (max)	$\sigma_{3\text{-}t2\text{-}max}$	24.924	mPa	where σ_{ext} is assumed to be zero
				Belyadi et al. (2019); Equation 13.14

Coulomb stress before 23.3 ka

Dip = 40°, Friction = 0.1				
Normal stress	σ_{n1}	31.315	MPa	$\sigma_n = \frac{\sigma_1 + \sigma_3}{2} - \frac{(\sigma_1 - \sigma_3)cos2\theta}{2}$
Shear stress	τ_1	5.318	MPa	
Coulomb stress	σ_{f1}	-4.144	MPa	Turcotte and Schubert (2019); Equation 2.58
Dip = 70°, Friction = 0.1				
Normal stress	σ_{n1}	26.241	MPa	$\tau = \frac{(\sigma_1 - \sigma_3)sin2\theta}{2}$
Shear stress	τ_1	3.471	MPa	
Coulomb stress	σ_{f1}	-2.804	MPa	
Dip = 40°, Friction = 0.7				Turcotte and Schubert (2019); Equation 2.57
Normal stress	σ_{n1}	31.315	MPa	
Shear stress	τ_1	5.318	MPa	
Coulomb stress	σ_{f1}	2.898	MPa	$\sigma_f = \mu(\sigma_n - P_p) - \tau$
Dip = 70°, Friction = 0.7				Harris (1998); Equation 1
Normal stress	σ_{n1}	26.241	MPa	
Shear stress	τ_1	3.471	MPa	
Coulomb stress	σ_{f1}	1.193	MPa	

Coulomb stress after 23.3 ka (10 m drop in water table)

Dip = 40°, Friction = 0.1

Normal stress	σ_{n2min}	31.279	MPa
Shear stress	τ_{2min}	5.301	MPa
Coulomb stress	$\sigma_{f2\text{-}min}$	-4.131	MPa

Dip = 70°, Friction = 0.1

Normal stress	σ_{n2min}	26.221	MPa
Shear stress	τ_{2min}	3.460	MPa
Coulomb stress	$\sigma_{f2\text{-}min}$	-2.796	MPa

Dip = 40°, Friction = 0.7

Normal stress	σ_{n2min}	31.279	MPa
Shear stress	τ_{2min}	5.301	MPa
Coulomb stress	$\sigma_{f2\text{-}min}$	2.889	MPa

Dip = 70°, Friction = 0.7

Normal stress	σ_{n2min}	26.221	MPa
Shear stress	τ_{2min}	3.460	MPa
Coulomb stress	$\sigma_{f2\text{-}min}$	1.190	MPa

Coulomb stress after 23.3 ka (33 m drop in water table)

Dip = 40°, Friction = 0.1

Normal stress	σ_{n2max}	31.198	MPa
Shear stress	τ_{2max}	5.264	MPa
Coulomb stress	$\sigma_{f2\text{-}max}$	-4.103	MPa

Dip = 70°, Friction = 0.1

Normal stress	σ_{n2max}	26.174	MPa
Shear stress	τ_{2max}	3.436	MPa
Coulomb stress	$\sigma_{f2\text{-}max}$	-2.777	MPa

Dip = 40°, Friction = 0.7

Normal stress	σ_{n2max}	31.198	MPa
Shear stress	τ_{2max}	5.264	MPa
Coulomb stress	$\sigma_{f2\text{-}max}$	2.869	MPa

Dip = 70°, Friction = 0.7

Normal stress	σ_{n2max}	26.174	MPa
Shear stress	τ_{2max}	3.436	MPa
Coulomb stress	$\sigma_{f2\text{-}max}$	1.181	MPa

SUMMARY OF COULOMB STRESS CHANGE CALCULATIONS

Water table drop of 10 m after 23.3 ka	$\Delta\sigma_f$	
Dip = 40°, Friction = 0.1	13	kPa
Dip = 70°, Friction = 0.1	8	kPa
Dip = 40°, Friction = 0.7	-9	kPa
Dip = 70°, Friction = 0.7	-4	kPa

Water table drop of 33 m after 23.3 ka	$\Delta\sigma_f$	
Dip = 40°, Friction = 0.1	41	kPa
Dip = 70°, Friction = 0.1	28	kPa
Dip = 40°, Friction = 0.7	-29	kPa
Dip = 70°, Friction = 0.7	-12	kPa

Notes

[1] Although it is convention to use depths of 5 km for Coulomb stress change calculations, here we use a depth of 2 km, which is based on seismic reflection data that shows that basement offset associated with the Eglington fault is located beneath about 2 km of Cenozoic alluvium (Langenheim et al., 1998).

[2] This range of values used here is in alignment with the default dip angle for normal faults in the USGS national seismic hazards model (Petersen et al., 2014).

[3] This is a minimum value that represents the pore pressure if the entire system was unconfined. In the Las Vegas Valley, however, there is a confining layer between the near-surface aquifer and the fault (the "blue clay" of Maxey and Jameson, 1948; Plume, 1989), so the actual pore pressure below this hydrologic barrier, while constant, is necessarily higher.